Theoretical Study of the Stereodynamics of CO Collisions with CH_3- and CF_3-Terminated Alkanethiolate Self-Assembled Monolayers†

William A. Alexander, John R. Morris, and Diego Troya*,†

Department of Chemistry, Virginia Tech, Blacksburg, Virginia 24061-0212

Received: December 1, 2008; Revised Manuscript Received: January 8, 2009

We present a classical-trajectory study of CO collisions with regular (CH_3-terminated) and ω-fluorinated (CF_3-terminated) alkanethiol self-assembled monolayers (SAMs) with a focus on analyzing the stereodynamics properties of the collision. The CO molecule is scattered with incident angles of either 30° or 60° with respect to the surface normal and with 60 kJ·mol^{-1} collision energy, and we analyze final translational and rotational energy, mechanism of the collisions, and orientation and alignment of the rotational angular momentum. Analysis of the alignment of the final rotational angular momentum in collisions involving initially rotationally cold CO indicates a slight preference for "cartwheel" and "corkscrew" rotational motions. In contrast, collisions of initially excited CO slightly favor "helicopter" motion of the recoiling molecule. Moreover, studies of final orientation reveal that, while cartwheel "topspin" motion is favored for collisions in which initially cold CO becomes rotationally excited, no preferred handedness is observed when CO leaves the surfaces with "helicopter" motion. Analysis of trajectories involving initially rotationally excited CO in which the initial rotational angular momentum is aligned and/or oriented shows a non-negligible effect of the initial rotational motion on the dynamics of energy transfer. For instance, CO approaching the SAMs with helicopter motion retains a larger fraction of its initial rotation than molecules colliding with cartwheel-type motions. Conservation of the alignment and orientation of the initial rotational angular momentum vector is also enhanced with helicopter motion relative to cartwheel or random motions. The calculated trends in the stereodynamic properties for the two SAMs indicate that the CH_3-SAM is effectively more corrugated than the CF_3-SAM.

I. Introduction

Studying energy transfer in collisions of gases with surfaces yields information important to a fundamental understanding of gas/surface chemical dynamics. In effect, gas/organic surface energy transfer is the essential first step in a variety of heterogeneous chemical reactions such as ozone depletion in the stratosphere,[1,2] degradation of satellite and spacecraft coatings in low-Earth orbit,[3,4] or the processing of organic aerosols,[5] to name a few. To thoroughly understand gas/organic surface energy transfer, it is necessary to determine the role played by the various degrees of freedom involved in the collision process, including not only the surface modes responsible for energy absorption and dissipation but also the translational, rotational, and vibrational modes of the scattering gas species. The role of the gas-phase species' translational energy in the absence of rovibrational influences has been elegantly investigated by many groups via molecular-beam and molecular-dynamics studies of rare gases colliding with organic liquids[6−9] and self-assembled monolayer (SAM) surfaces,[10−25] and of oxygen atom collisions with these surfaces.[26−29] Early efforts in atomic scattering from low-vapor pressure liquids such as squalane and perfluoropolyether (PFPE) revealed that, in many cases, the dynamics of gas/organic surface collisions can be understood as a competition between two main mechanisms: impulsive scattering and thermal desorption.[6−9] The thermal-desorption component refers to collisions in which the impinging gas-phase species loses enough energy to thermalize with the surface before desorbing with a Boltzmann distribution of energies at the surface temperature. In contrast, impulsive scattering events are characterized by brief encounters with the surface that most often limit energy transfer and thermalization, resulting in a second, high-energy component in the final translational energy distributions. Comparison of the scattering properties of rare gases from squalane and PFPE revealed a critical dependence on liquid composition,[6,7] and subsquent studies showed surface roughness to play an important role in the scattering dynamics.[30]

The use of SAMs as model organic surfaces in studies of gas/surface collisions allows control over the supramolecular structure of the surface and its interfacial chemical characteristics. Pioneering studies by Cohen et al. in the late 1980s posited that the most important factors governing the collision dynamics of a particular gas with a SAM are (1) mass of the SAM terminus and (2) energy disposal into low-frequency, high-amplitude modes of the SAM.[31,32] Subsequent studies have probed the influence that SAM terminal groups,[10,11,15−17] SAM packing density,[12,14] potential-energy surface considerations,[13,15,20] and incident gas identity[15,21−23,33] have on the scattering dynamics.

In comparison to monatomic gas/organic surface scattering, studies involving the scattering of small polyatomic gas-phase species from organic surfaces are not as abundant.[8,31−46] In addition, only a few of these studies have been able to investigate state-to-state energy transfer by resolving the rovibrational state populations of the recoiling gas species. State-resolved studies include those of Cohen et al., who scattered O_2 and NO from SAMs,[31,32] Kenyon et al., who scattered I_2 from liquids,[34,35] Perkins and Nesbitt, who investigated CO_2 scattering off squalane and PFPE,[37−41] and Bagot et al., who measured OH scattering properties from those same two organic

† Part of the "George C. Schatz Festschrift".

* Corresponding author, troya@vt.edu.

10.1021/jp810557m CCC: $40.75
Published on Web 02/10/2009

liquids.[45] A collective conclusion of these studies was that the same two limiting impulsive-scattering and thermal-desorption mechanisms invoked to understand atomic scattering also apply to molecular scattering from organic surfaces. In the case of molecular scattering, this has been shown not only by analysis of the recoil energy of the gas molecules but also by measurement of their internal-state distributions, in particular rotational distributions. The surface governs the competition between these two limiting mechanisms for a particular gas molecule, with fluorinated surfaces generally inducing more direct processes than hydrogenated surfaces.

An exciting new development in the quantum state resolved gas/organic liquid experiments mentioned above has been aimed at elucidating the stereodynamic properties of CO_2/PFPE collisions.[40] Use of differential absorption characteristics of circularly polarized light has revealed that CO_2 preferentially scatters from the surface with a forward end-over-end topspin orientation, an effect that is enhanced as the final rotational state increases. Complementary molecular dynamics simulations of CO_2 scattering from perfluorinated SAMs were shown to agree with the experimentally observed orientational preference. To the best of our knowledge, this is the first time that stereodynamic effects have been measured in gas/organic surface scattering. In contrast, analogous studies involving metal surfaces are prevalent in the literature.[47−54] Of particular relevance to the work presented herein are the studies of Hanisco et al. of CO scattering from the Ag(111) surface.[47,48] In that work, resonantly enhanced multiphoton ionization (REMPI) spectroscopy was used to investigate the influence of collision with the Ag surface on CO's final angular momentum alignment. A supersonic beam of rotationally cold (T_{ROT} < 5 K) CO was directed onto the Ag surface along the surface normal with ~72 kJ·mol^{-1} collision energy, and the alignment of the rotational angular momentum of the backscattered CO was measured. While no efforts were taken to initially align the impinging CO molecules, cartwheel motion, in which the CO rotates in a plane perpendicular to the surface plane, was found to be preferred in the scattered flux, with the extent of alignment ranging from near zero for rotationally cold CO to up to 90% for high (j' > 20) rotational states. The extent of alignment was also shown to increase with increasing collision energy. While scattering from Ag results in aligned CO molecules for high rotational energy levels, N_2 scattering at the same initial conditions showed pure cartwheel alignment for final rotational states as low as j' = 12. The differences in the alignment of CO relative to N_2 were attributed to the greater anisotropy of the CO/Ag potential energy surface relative to N_2/Ag. The interactions between the departing CO and the corrugated surface potential act to steer the departing molecules away from the perfect cartwheel alignment that would otherwise result from an isotropic gas/surface potential.

In a previous effort, our group has investigated collisions of CO with CH_3- and CF_3-SAMs to probe the influence of incident energy, angle, and rovibrational state on the scattering dynamics.[36] Our results generally paralleled those of Nesbitt et al. on CO_2/liquid systems and additionally indicated that polyatomic scattering cannot adequately be described by simple kinematic models of gas/surface scattering in which the gas species is approximated by a structureless particle. In this work, we extend our study of CO scattering from CH_3- and CF_3-SAMs by examining collisional stereodynamics via classical-trajectory simulations. Our results are examined in reference to the previous CO/Ag work and will be compared to the recent work on CO_2/liquid systems to further our understanding of how surface corrugation influences gas/surface collision dynamics.

II. Computational Details

The potential-energy surfaces used to evolve the CO/SAM trajectories are analogous to those employed in our prior work on rare gas/SAM collisions.[13−15] In those studies, we divided the global potential into two terms: the potential describing the organic monolayer (surface potential) and the potential for the interactions between the gas and the SAM (gas/surface potential). In this work, we add a third term to the global potential to describe the CO molecule (gas potential). All three terms of the potential-energy surface in our CO/SAM simulations have been fully described in our prior work on this system;[36] therefore, we present here only a brief summary of each part of the potential.

First, a hybrid explicit atom/united atom OPLS force field[55−57] is used for the surface potential. This standard force field bears out the experimental structure of the SAMs, including a 30° tilt of the chains,[58] and provides good agreement with experiment in scattering simulations of rare gases with SAMs.[13−15] Second, CO is described using a standard Morse function with parameters chosen so that the calculated spectroscopic constants of CO agree with experiment. Third, the gas/surface potential is described using two-body Buckingham potentials derived from highly accurate ab initio calculations of CO/hydrocarbon pairs.[36,59] Specifically, the intermolecular energies of CO in various approaches to the CH_4 and CF_4 molecules were calculated at the focal-point coupled-cluster with single, double, and perturbative triple excitations level with extrapolation to the complete basis set limit [fp-CCSD(T)/CBS]. These high-quality points of the intermolecular potential-energy surface were then used to fit pairwise Buckingham potentials, which can be conveniently employed to propagate CO/SAM trajectories.

Using the analytical potential-energy surfaces, we have performed classical-trajectory calculations of collisions of the CO molecule with both regular (CH_3-terminated) and ω-fluorinated (CF_3-terminated) alkanethiol self-assembled monolayers. These SAMs are composed of 36 thiolate chains ($S-(CH_2)_{11}-CH_3$ or $S-(CH_2)_{11}-CF_3$ for CH_3- and CF_3-SAMs, respectively) that are replicated in the two axes of the surface plane using the periodic-boundary-conditions algorithm of the TINKER package of programs.[60] The chains are arranged in a hexagonal pattern, and are separated by 4.98 Å. These geometrical parameters mimic the structure of SAMs on a Au(111) surface. However, to simplify the calculations, we have not included the Au(111) surface explicitly; instead, we have held the sulfur atoms of the SAM chains fixed in their minimum-energy locations on a Au(111) surface throughout the scattering calculations.

We have integrated batches of trajectories with various initial conditions, including 60 kJ·mol^{-1} collision energy (E_{coll}), CO(v = 0, j = 0) or CO(v = 0, j = 28) rovibrational states and 30° or 60° angles of incidence (θ_i). In addition, CO either has been initially given a random collision geometry or assigned a specifically aligned/oriented approach geometry. The specifics of these initial collision geometries will be elaborated below. For random collision geometry, 10000 trajectories have been calculated for each combination of surface, incident angle, and initial CO rotational state, and for the aligned/oriented approaches, 2000 trajectories have been calculated for the same combinations. Overall, 136000 trajectories have been calculated in this work. Initial conditions for the CO molecule have been determined via quasi-classical sampling of selected vibrational

and rotational states as implemented in the VENUS96 computer program.[61] At the beginning of each trajectory, CO has been placed above the surface at a separation of at least 10 Å from the closest surface atom. The initial conditions (coordinates and momenta) of the surface have been taken as intermediate steps of a 0.5 ns canonical simulation of the SAM at 300 K. The initial azimuthal angle formed by the incident CO velocity vector and the tilt direction of the SAM chains has been randomly selected.

The trajectories have been stopped postcollision either when the gas recoiled to a distance of 12 Å from the closest atom of the surface or, in the case of long-trapping processes, if the CO molecule has not desorbed from the surface after 15 ps. The trajectories terminated as a result of long trapping times were assumed to be fully thermalized with the surface and were randomly assigned final translational energy, E'_T, and rovibrational states v' and j' based on Boltzmann distributions at the surface temperature. However, since the degree of orientation and alignment of the final CO rotational angular momentum in these long-trapped trajectories cannot be predicted a priori, we have not included trajectories in which CO does not desorb the surface within our 15 ps time cutoff in the analysis of orientation and alignment of the final rotational angular momentum.

From the initial and final coordinates and momenta of the CO molecule, scattering properties including product translational energy distributions, CO rotational state distributions, and alignment and orientation of the CO final rotational angular momentum with respect to various axes have been determined. Examination of CO's coordinates and momenta during the trajectories has been used to gain insight into the mechanism of energy exchange during the collisions.

III. Results and Discussion

A. Collision Dynamics of CO in the $v = 0, j = 0$ State. ***1. Energy Transfer.*** Full details of the scalar properties of gas/surface energy tranfer in CO/SAM collisions have been published elsewhere.[36] Therefore, here we provide only a brief discussion of the results that are essential to understand the stereodynamic properties of the collisions that we describe later.

Figure 1a shows the calculated product translational energy distributions of CO after collision with CH_3- and CF_3-SAMs at $E_{coll} = 60$ kJ·mol^{-1} and with incident angles of 30° and 60°. The average energies of these distributions are listed in Table 1 ($\langle E'_T \rangle$). The data in the figure and table reveal that energy transfer from CO translation is very efficient in collisions with both surfaces, with the CH_3-SAM being a better energy absorber than the CF_3-SAM; at $\theta_i = 30°$, CO loses ~87% and ~75% of its translational energy in collision with the CH_3- and CF_3-SAMs, respectively. The distinct behavior of both surfaces seems even more pronounced at grazing incident angles: with $\theta_i = 60°$, CO loses ~73% and ~52% of its translational energy in collision with the same surfaces. The differential energy transfer behavior in collisions with these two surfaces has been examined in detail elsewhere[36] and agrees with recent rare-gas scattering results from the same surfaces.[15] The previous studies determined that surface mass controls the differences between these two SAMs and that the more massive surface impairs energy transfer from the impinging gas-phase projectile.[15,36] Another important result is that more grazing collisions cause CO to lose less energy to the surfaces, as can be expected from the notion that the gas species' momentum parallel to the surface is better conserved than its perpendicular momentum.

Table 1 shows additional information about the scattering process, including energy transfer to CO rotational degrees of freedom. The calculations reveal that CO becomes more rotationally excited when scattering from the CF_3-SAM than from the CH_3-SAM, which is consistent with the larger rigidity of the heavier SAM. Increasing the incident angle from 30° to 60° results in little change in final rotational excitation. This is an interesting result, because in contrast, average CO final translational energies double on both surfaces. Figure 1b shows the full rotational distributions of CO for the four combinations of surface and incident angle calculated in this work. The figure cleanly shows the larger rotational excitation gained by CO in collisions with the CF_3-SAM surface in comparison with the CH_3-SAM surface and the mild effect of the incident angle. With respect to vibrational energy transfer, all of the collisions are seen to be vibrationally adiabatic, irrespective of initial vibrational ($v = 0$ or 1) or rotational ($j = 0-28$) excitation.

Regarding the collision mechanism, we list in Table 1 two indicators that help capture the broader aspects of the pathways followed by CO scattering from the SAMs studied here. First, we show the percentage of trajectories that experience only one encounter with the surface (% direct in Table 1). In this paper, we consider that a trajectory exhibits a direct mechanism when the CO center-of-mass coordinate along the surface-normal axis has only one turning point during the collision. Second, we show

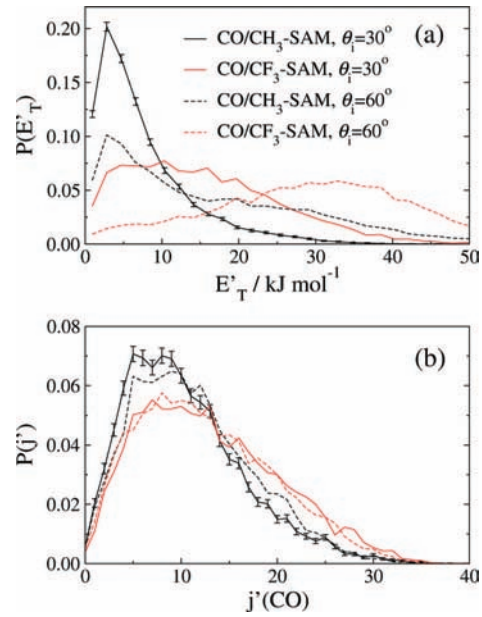

Figure 1. Calculated (a) product translational energy distributions and (b) final rotational state distributions in collisions of CO with CH_3- and CF_3-SAMs at $E_{coll} = 60$ kJ·mol^{-1} with $\theta_i = 30°$ and 60°. The distributions are normalized to unit area.

TABLE 1: Energy Transfer Properties in Collisions of CO($v = 0, j = 0$) with CH_3- and CF_3-SAMs[a]

surface	θ_i	$\langle E'_T \rangle$[b]	$\langle E'_{ROT} \rangle$[c]	% direct[d]	% long[e]
CH_3-SAM	30	7.7	3.4	39.0	30.5
	60	16.3	3.7	48.4	18.9
CF_3-SAM	30	15.5	5.1	74.7	6.7
	60	29.3	4.7	72.5	2.7

[a] 60 kJ·mol^{-1} collision energy. [b] Average final CO translational energy in kJ·mol^{-1}. [c] Average final CO rotational energy in kJ·mol^{-1}. [d] Percentage of trajectories experiencing only one turning point. [e] Percentage of trajectories in which CO does not desorb the surface after 15 ps. Conservative estimates of the sampling error in average translational and rotational energies are 0.7 and 0.4 kJ·mol^{-1}, respectively. Estimated errors in the "direct" and "long" precentages are 2.0 and 0.5%, respectively. These estimated errors are applicable for these quantities throughout this study.

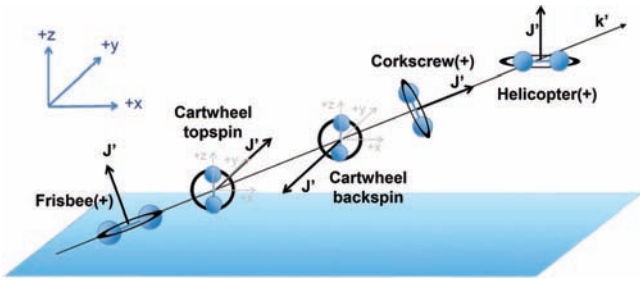

Figure 2. Schematic of the various limiting rotational motions of a diatomic molecule scattering from a surface. Two orientations are shown for the cartwheel alignment.

the percentage of trajectories in which CO does not desorb from the SAM surface after 15 ps (% long in Table 1). The values of these scattering properties show that direct scattering is notably larger for the fluorinated SAM than for the regular SAM. On the other hand, long trapping on the surface is much larger for the CH_3-SAM. These results are clearly reflective of the well-known larger rigidity of the terminally fluorinated SAM.

In summary, various dynamics properties indicate that the CF_3-SAM is a more rigid collision partner than the CH_3-SAM. This effect results in less translational energy transfer to the surface, more transfer to CO rotational energy, more direct collisions, and less long trapping for the CF_3-SAM than for the CH_3-SAM. In addition, more grazing collisions result in decreased translational energy transfer to the surface but do not affect substantially the amount of energy channeled into CO rotation. More grazing incidence also enhances direct collisions and diminishes long trapping on the surface.

2. Alignment and Orientation of the Final CO Rotational Angular Momentum. We now investigate how the collision of CO($v = 0$, $j = 0$) with a SAM drives rotational angular momentum alignment and orientation of the recoiling CO molecule. As mentioned in the introduction, some experiments can obtain information about the plane of rotation of a linear molecule (alignment)[51] and the handedness of the rotation (orientation).[40] However, simultaneous determination of both alignment and orientation is extremely difficult,[62] and this usually impairs a complete understanding and quantification of the type of rotational motion of the gas species after collision with a surface.

The ultimate goal of stereodynamics studies is to elucidate the exact type of rotational motion that a molecule possesses after collision with a surface and connect this information with the gas/surface interaction. There are various limiting types of rotational motion with which a diatomic molecule can leave a surface. In terms of alignment, one can define four limiting rotational motions: cartwheel, helicopter, corkscrew (also termed propeller), and frisbee. A schematic of these rotational motions is depicted in Figure 2 and video files of actual trajectories that exhibit these motions can be found in the Supporting Information. As shown in the figure, the four limiting motions can be defined considering the relationship between the final rotational angular momentum of the molecule, $\mathbf{J}'$, and the final center-of-mass velocity vector, $\mathbf{k}'$, or the surface normal, $\mathbf{z}$, in the case of helicopter motion. Alignment studies give insight into the plane in which the molecule rotates but provide no information about the orientation or handedness of the rotation (clockwise or counterclockwise, exemplified in Figure 2 by the topspin and backspin orientations possible in the limiting case of cartwheel alignment). Complete stereodynamics studies require determination of both the preferred alignment and orientation of the rotation. While, as mentioned before, simultaneous determination of alignment and orientation by experimental means is complicated, molecular-dynamics simulations can provide information of both alignment and orientation of gas-phase molecules after collision with a surface. This makes atomistic simulations an attractive tool to enhance our understanding of gas/surface dynamics.[52,54,63−65]

In an effort to establish comparison between our calculations on the CO/SAM system and earlier measurements on CO/metal and CO_2 /liquid systems, we show in Table 2 CO final rotational angular momentum orientation and alignment moments after collision with a SAM that can, in principle, be measured in an experiment. In classical mechanics, orientation moments can be calculated by obtaining the projections, J'_i, of the rotational angular momentum vector $\mathbf{J}'$ on each of the axes of a frame of reference. In this work, we define a Cartesian frame of reference in the conventional way, i.e., by locating the SAM surface in the xy-plane and scattering CO in the xz-plane (see Figure 2). In this Cartesian frame, the CO molecule is moving away from the surface after collision with positive velocity components in the z- and x-axis if the molecule scatters forward (the x-velocity component might be negative if CO recoils backward). (Note that in experiments, in-plane scattering is usually measured exclusively, but in this work we examine all of the CO flux, including out-of-plane trajectories. However, we have verified that out-of-plane scattering is not highly probable in the calculations, so the results presented here are mostly due to in-plane scattering.) With this reference frame in mind, average $J'_i/|\mathbf{J}'|$ values provide information about the preferred handedness of the rotation (clockwise or counterclockwise) with respect to the specific i-axis. $+1.0$ or -1.0 values of the $J'_i/|\mathbf{J}'|$ ratio indicate exclusive handedness, and a value of 0.0 indicates no overall handedness. These calculated $J'_i/|\mathbf{J}'|$ factors are the classical analogues of the $A_1^{\{1\}}$ moment of the rotational angular momentum polarization distribution,[62] which is commonly reported in the experiment. On the other hand, average $3J'^2_i/|\mathbf{J}'|^2 - 1$ values provide information about alignment. A value of $+2.0$ for the $3J'^2_i/|\mathbf{J}'|^2 - 1$ alignment factor indicates that the molecule is exclusively rotating in a plane perpendicular to the i-axis. A value of -1.0 indicates rotation in a plane parallel to the i-axis, and a value of 0.0 indicates no preferred plane of rotation with respect to that axis. These calculated $3J'^2_i/|\mathbf{J}'|^2 - 1$ factors are the classical analogues of the popular $A_0^{\{2\}}$ moment of the rotational angular momentum polarization distribution that has been measured in various experiments, especially with respect to the z-axis (surface normal).[62]

The calculated average orientation and alignment moments calculated in this way are shown in Table 2. When the moments are calculated taking into consideration all of the CO flux (regardless of its final rotational excitation), their values are close to zero, suggesting that overall, rotational angular momentum polarization is weak in CO/SAM collisions. However, the situation changes when one performs the analysis for CO molecules that become highly rotationally excited ($j' \geq 20$) as a result of the collision with the SAM surfaces (values in parentheses in Table 2). For instance, the values of the $3J'^2_y/|\mathbf{J}'|^2 - 1$ moment are significantly larger than 0.0, which indicates a tendency of the CO molecule to rotate in the xz-plane (cartwheel rotation). This tendency toward cartwheel rotation is enhanced with more grazing collisions and for the heavier surface. In addition, the average values of $J'_y/|\mathbf{J}'|$ (orientation moment) are also significantly larger than 0.0, indicating a preferred handedness in the cartwheel rotation. This preferential handedness also increases with a more grazing incident angle but does not depend very strongly on the surface.

TABLE 2: Average Orientation and Alignment Moments of the Final Rotational Angular Momentum in Collisions of CO($v = 0, j = 0$) with CH_3- and CF_3-SAMs at $E_{coll} = 60$ kJ·mol^{-1}[a]

surface	θ_i	$\langle J'_x\rangle/(\|\mathbf{J}'\|)$	$\langle 3J'^2_x\rangle/(\|\mathbf{J}'\|^2) - 1$	$\langle J'_y\rangle/(\|\mathbf{J}'\|)$	$\langle 3J'^2_y\rangle/(\|\mathbf{J}'\|^2) - 1$	$\langle J'_z\rangle/(\|\mathbf{J}'\|)$	$\langle 3J'^2_z\rangle/(\|\mathbf{J}'\|^2) - 1$
CH_3−SAM	30	−0.01 (0.02)	0.00 (−0.04)	0.04 (0.18)	0.05 (0.11)	0.00 (0.02)	−0.04 (−0.08)
	60	0.00 (−0.02)	−0.03 (−0.04)	0.06 (0.23)	0.10 (0.22)	−0.02 (−0.01)	−0.07 (−0.18)
CF_3−SAM	30	0.01 (0.01)	−0.03 (0.01)	0.04 (0.11)	0.06 (0.24)	0.00 (0.01)	−0.02 (−0.24)
	60	−0.01 (−0.04)	0.00 (0.01)	0.08 (0.26)	0.11 (0.33)	−0.01 (−0.02)	−0.11 (−0.33)

[a] Values in parentheses correspond to averages over trajectories in which CO results with a final rotational quantum number of 20 or larger. Conservative estimates of the sampling error in the orientation and alignment moments are 0.06 and 0.09, respectively. These estimated errors are applicable for these quantities throughout this study.

In this work, positive values of $J'_y/|\mathbf{J}'|$ represent topspin rotation (see Figure 2). Therefore, the results in Table 2 suggest that cartwheel topspin rotation is slightly favored for highly rotationally excited CO.

A second result of interest in Table 2 is the presence of slight alignment with respect to the z-axis (surface normal). The average values of $3J'^2_z/|\mathbf{J}'|^2 - 1$ for rotationally excited CO show a small but noticeable deviation from 0.0 toward negative values. These results suggest a slight tendency for CO to avoid rotation in the SAM surface plane, which would correspond to helicopter motion. Instead, CO has a propensity to rotate in a plane containing the z-axis. Depending on the recoil angle, there are various motions that could satisfy this result, including cartwheel, which is consistent with the positive values of $3J'^2_y/|\mathbf{J}'|^2 - 1$, but also corkscrew, if the CO molecule is recoiling in a direction near-parallel to the SAM surface (see Figure 2).

The presence of cartwheel alignment in our CO/SAM calculations agrees with the results of CO scattering from Ag(111).[48] Indeed, cartwheel alignment is the expected result for a homonuclear diatomic gas-phase species scattering from a flat, smooth surface, since the gas/surface forces that lead to rotational excitation are exclusively in the direction normal to the surface. This idealized surface model also predicts that the larger the rotational excitation, the larger the cartwheel alignment will be. With this model in mind, departure from pure cartwheel alignment in gas/surface scattering is an indication of the magnitude of tangential forces. These forces along the x- and y-directions can be traced to the corrugation of the surface (and therefore the gas/surface potential) so that the further the alignment is from pure cartwheel, the more corrugated the surface is. Whereas in the measurements of CO scattering from Ag(111) (normal incidence, $E_{coll} \sim 72$ kJ·mol^{-1}), the $3J'^2_z/|\mathbf{J}'|^2 - 1$ alignment moment was approximately −0.9 for $j' = 25$ and larger, the most negative $3J'^2_z/|\mathbf{J}'|^2 - 1$ value obtained here is −0.33 for CO/CF_3-SAM collisions with $\theta_i = 60°$ and $E_{coll} = 60$ kJ·mol^{-1} for which the final rotational quantum state of CO is 20 or larger. This comparison of alignment moments with respect to the surface normal clearly shows that the SAM surfaces used in this work are much more corrugated than the Ag(111) metal surface.

Regarding orientation, while the CO experiments on silver did not report orientation moments, recent simulations by Perkins and Nesbitt of CO_2 scattering from a fully fluorinated SAM at $E_{coll} = 43$ kJ·mol^{-1} and $\theta_i = 60°$, performed to accompany experiments of CO_2 scattering from a perfluorinated liquid surface, reported an increased tendency toward topspin vs backspin orientation by calculating $J'_y/|\mathbf{J}'|$ ratios.[40] Specifically, while CO_2 scattering with $j' < 10$ does not show any orientational preference, up to ∼30% of trajectories in which CO_2 scatters with $j' > 50$ have $J'_y/|\mathbf{J}'|$ values between 0.8 and 1.0. In an attempt to compare our results directly with those of CO_2 scattering from perfluorinated SAMs, we show in Figure 3 the evolution of the distribution of $J'_y/|\mathbf{J}'|$ orientation moments as a function of the level of rotational excitation in CO after collision with the CH_3- and CF_3-SAM at the two incident angles examined in this work. As can be seen in Figure 3, at low values of j', the $J'_y/|\mathbf{J}'|$ distributions are largely isotropic for both surfaces at both angles, implying no orientational preference. As j' increases, the distributions shift toward positive values of $J'_y/|\mathbf{J}'|$, indicating that CO scattering with large rotational excitation preferentially emerges with a topspin orientation. This result parallels the circular polarizance measurements of CO_2 scattering from PFPE and is in good agreement with molecular dynamics simulations of CO_2 scattering from a perfluorinated SAM at $E_{coll} \sim 43$ kJ·mol^{-1} and $\theta_i = 60°$.[40] In fact, our calculations for CO/CF_3-SAM scattering at $\theta_i = 60°$ also yield approximately 30% of the trajectories having $J'_y/|\mathbf{J}'|$ values between 0.8 and 1.0 (Figure 3d). In an idealized model of a rotationless diatomic molecule undergoing collision with a flat, smooth surface exerting force only along the surface normal direction, symmetric topspin−backspin orientation would be expected. In addition, since momentum perpendicular to the surface normal is conserved in this ideal case, the orientational symmetry is preserved for all angles of incidence. The origin of this symmetry emerges from the equiprobable sampling of initial collision geometries in which the nonrotating diatomic axis is tilted up or down with respect to the surface normal. If the molecular axis is tilted up toward the surface normal, the trailing atom in a glancing approach collides first with the surface, and the subsequent torque from the repulsion in the surface-normal direction causes forward tumbling (topspin motion). Conversely, if the molecular axis prior to collision is tilted down, the leading atom collides first with the surface, and the torque experienced by the molecule causes it to tumble backward (backspin motion). If the initial sampling of collision geometries is entirely random, the number of collisions in which the diatomic axis is tilted up or down prior to collision is identical, and therefore topspin−backspin symmetry should be expected. With this model in mind, the departure from topspin−backspin symmetry in the cartwheel alignment seen in this work is therefore indicative of the presence of gas/surface forces in directions other than the surface normal. In-plane gas/surface repulsions in the direction of travel will favor topspin rotation, and this is exactly what is observed in our calculations, as reflected in the $J'_y/|\mathbf{J}'|$ values of Table 2 and Figure 3.

As mentioned before, Table 2 contains rotational angular momentum polarization moments that could be obtained in an experiment. While the analysis of the listed orientation and alignment moments reveals interesting information about the rotational motion of CO scattering from a SAM, an understanding of the precise types of motions and their handedness is limited using only those data. For instance, the contributions of corkscrew and frisbee motions cannot be determined from the data in the table because, unlike the helicopter and cartwheel motions, these motions are not defined with respect to the chosen Cartesian reference frame, but with respect to the final velocity

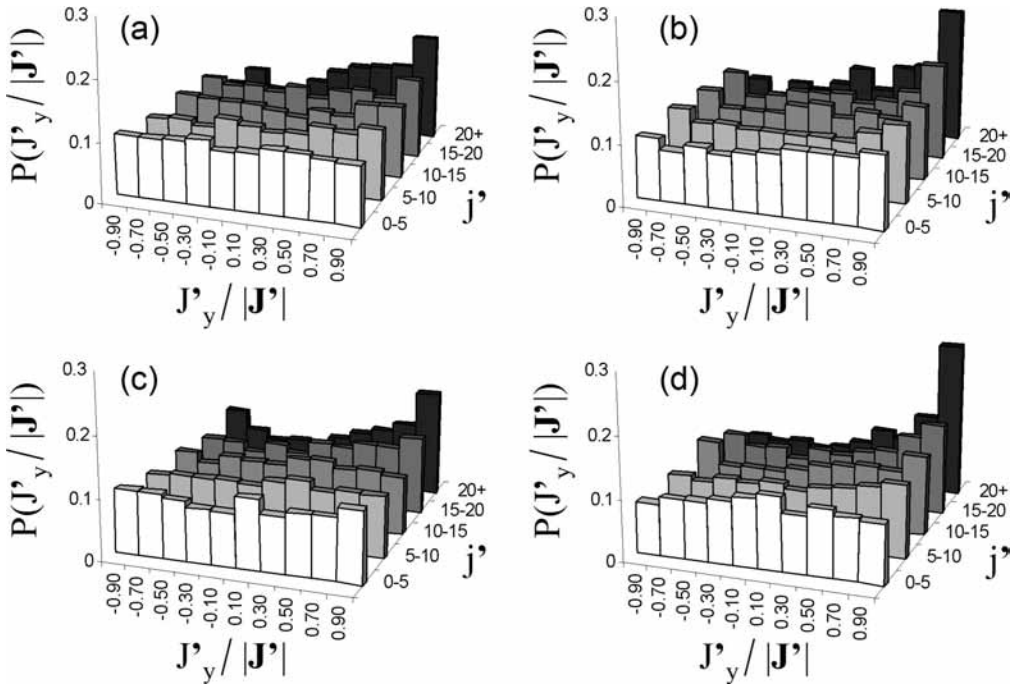

Figure 3. Calculated $J'_y/|\mathbf{J}'|$ distributions as a function of final rotational state for CO($v = 0, j = 0$) scattering with either $\theta_i = 30°$ (a and c) or $\theta_i = 60°$ (b and d) from the (a, b) CH_3- and (c, d) CF_3-SAM surfaces.

vector $\mathbf{k}'$. Therefore, a knowledge of $\mathbf{k}'$, i.e., the final polar-angle distribution, is necessary to investigate the presence of corkscrew or frisbee rotation. Since the negative values of $3J'_z{}^2/|\mathbf{J}'|^2 - 1$ (see Table 2) reveal that helicopter type scattering is negligible, we focus on analyzing our trajectory data in a way that will lead us to the determination of the relative contributions of cartwheel, corkscrew, and frisbee motions and their handedness. This analysis is performed by calculating the angles between the final center-of-mass velocity of CO ($\mathbf{k}'$), the surface normal ($\mathbf{z}$), and the rotational angular momentum ($\mathbf{J}'$) vectors.

Corkscrew-type motion occurs when the angle between the final CO rotational angular momentum vector $\mathbf{J}'$ and the final CO center of mass velocity vector $\mathbf{k}'$ is either 0° or 180° (see Figure 2). On the other hand, frisbee motion occurs when the $\mathbf{k}'$ and $\mathbf{J}'$ vectors are perpendicular. In cartwheel motion, $\mathbf{k}'$ and $\mathbf{J}'$ are also perpendicular. Since frisbee and cartwheel alignments are indistinguishable via examination of only the $\mathbf{k}'\mathbf{J}'$ angle, a second angle involving $\mathbf{J}'$ must be introduced to differentiate these two motions. In this work, we distinguish between frisbee and cartwheel motion by examining the angle between $\mathbf{J}'$ and a vector normal to the plane defined by the SAM surface normal vector $\mathbf{z}$ and $\mathbf{k}'$. (Recall that the $\mathbf{z}$ vector starts in the sulfur plane of atoms and points away from the SAM, i.e., in the $+z$ direction, as noted in Figure 2.) The vector normal to the plane defined by the $\mathbf{z}$ and $\mathbf{k}'$ vectors is calculated as the cross product of these two vectors and will be referred to in this paper as $\mathbf{z} \times \mathbf{k}'$. Assuming that the SAM surface is in the xy-plane and that the recoiling CO molecule travels in the xz-plane with positive velocities in both the x- and z-axes, the vector $\mathbf{z} \times \mathbf{k}'$ is parallel to the y-axis and points toward the $+y$ direction. With this definition of the $\mathbf{z} \times \mathbf{k}'$ vector, we can distinguish cartwheel and frisbee motions by examining the angle formed by the $\mathbf{z} \times \mathbf{k}'$ and $\mathbf{J}'$ vectors. If the $(\mathbf{z} \times \mathbf{k}')\mathbf{J}'$ angle is 90°, then the motion is pure frisbee, and if the $(\mathbf{z} \times \mathbf{k}')\mathbf{J}'$ angle is 0° or 180°, the motion is pure cartwheel (see Figure 2).

With the angular analysis described above, one can also readily determine the handedness (orientation) of the corkscrew and cartwheel motions. In the corkscrew+ (clockwise) rotation, the $\mathbf{k}'\mathbf{J}'$ angle is 0°, and in the corkscrew− (counterclockwise) rotation, the $\mathbf{k}'\mathbf{J}'$ angle is 180°. Analogously, in the cartwheel topspin rotation, the $(\mathbf{z} \times \mathbf{k}')\mathbf{J}'$ angle is 0°, and in the cartwheel backspin rotation the $(\mathbf{z} \times \mathbf{k}')\mathbf{J}'$ angle is 180°. With these considerations in mind, the probability of the various types of rotational motion of CO recoiling from SAMs can be elucidated by examining the probability distributions of the $(\mathbf{z} \times \mathbf{k}')\mathbf{J}'$ and $\mathbf{k}'\mathbf{J}'$ angles.

Figure 4 shows contour plots for the probability of the recoiling CO molecules simultaneously having given $(\mathbf{z} \times \mathbf{k}')\mathbf{J}'$ and $\mathbf{k}'\mathbf{J}'$ angles in collisions with SAMs at $E_{coll} = 60$ kJ·mol^{-1}. CO is initially in its ground rovibrational state ($v = 0, j = 0$) before collision. Figure 4a displays the results for a CH_3-SAM with a 30° incident angle. The plot reveals small probability peaks in the $\cos(\mathbf{k}'\mathbf{J}') = 0.0$ and $\cos((\mathbf{z} \times \mathbf{k}')\mathbf{J}') = +1.0$ and -1.0 regions, which correspond to cartwheel topspin and backspin motions, respectively. These peaks have roughly the same intensity, indicating that topspin or backspin motions are nearly equally probable. Peaks in the regions of the graph corresponding to corkscrew+ and corkscrew− rotational motions ($\cos((\mathbf{z} \times \mathbf{k}')\mathbf{J}') = 0.0$ and $\cos(\mathbf{k}'\mathbf{J}') = +1.0$ or -1.0, respectively) are also appreciable, but their intensities are even smaller than those corresponding to cartwheel motions. There is no evidence for frisbee rotation. The probabilities for cartwheel, and especially corkscrew motions, are accentuated when CO impinges on the same surface at 60° (Figure 4b). In addition, at this incident angle cartwheel topspin rotation seems slightly more favored than backspin rotation. This result indicates that more grazing collisions seem to provide enhanced alignment and orientation of the CO rotational angular momentum.

Much as in the case of the CH_3-SAM, the probability contours in CO/CF_3-SAM collisions at $\theta_i = 30°$ also show a peak in the cartwheel and corkscrew regions (Figure 4c). However, the intensity of the peaks in the corkscrew direction is comparable to those in the cartwheel regions. The description of the preferred alignment of CO's final rotational angular momentum is substantially different for collisions at 60° on the same CF_3-SAM surface (Figure 4d) in three key ways. First, as with the CH_3-SAM results, the graph is

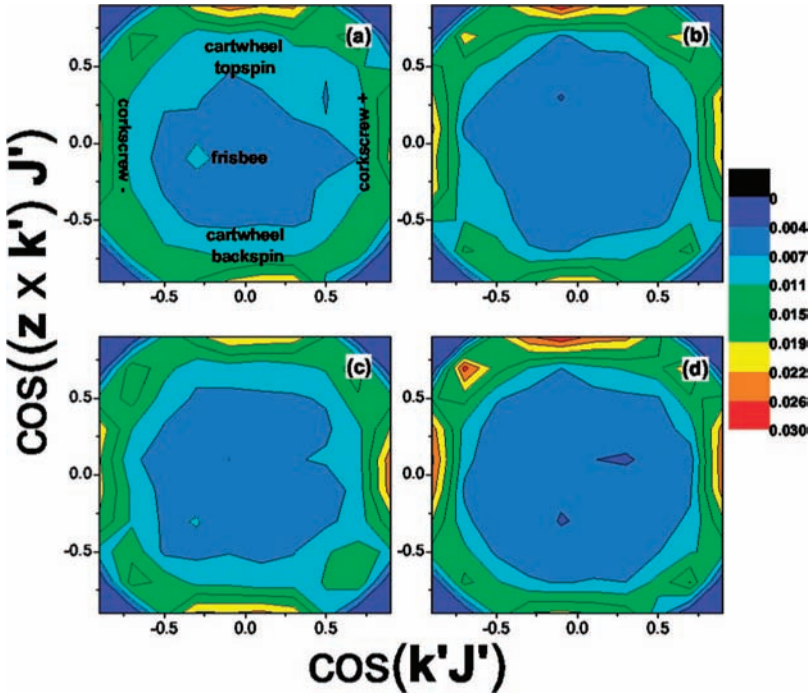

Figure 4. Probability contours of CO scattering with given $\mathbf{k}'\mathbf{J}'$ and $(\mathbf{z} \times \mathbf{k}')\mathbf{J}'$ angles in collisions with a CH_3-SAM (a), (b), and a CF_3-SAM (c), (d), at $E_{coll} = 60$ kJ·mol^{-1} and $v = 0$, $j = 0$. The angle of incidence is 30° for (a) and (c) and 60° for (b) and (d). Contours are drawn from zero probability (blue) to probability 0.03 (maroon) at 0.00375 steps. Labels in panel a indicate the location of the limiting rotational motions.

more anisotropic at $\theta_i = 60°$, corroborating the idea that more grazing collisions enhance alignment. Second, there is a propensity toward cartwheel topspin over cartwheel backspin motion. The difference in the intensities of the topspin and backspin peaks is slightly larger than with the CH_3-SAM, suggesting that the heavier surface also enhances orientation. Finally, the cartwheel topspin peak is larger than the corkscrew peaks, which contrasts with the similar intensities seen at $\theta_i = 30°$ on the same CF_3-SAM surface.

The emerging picture from Figure 4 is that when rotationally cold, but translationally hot, CO approaches a SAM surface with random collision geometry, scattered rotationally excited CO shows a weak but non-negligible degree of cartwheel and corkscrew alignment after collision. Alignment is increased for more grazing collisions and for the heavier surface, which also favors topspin vs backspin orientation for cartwheel scattering.

Table 2 shows that both orientation and alignment are enhanced for rotationally excited CO. To verify this effect, we present in Figure 5 contour plots similar to those in Figure 4, but constructed with trajectories in which CO scatters with a final rotational quantum number $j' \geq 20$. The probability contour plots obtained with CO having high rotational excitation are notably more anisotropic than those considering all of the CO flux, suggesting that alignment and orientation of the rotational angular momentum is indeed enhanced if the rotational angular momentum is large. Aside from the larger anisotropy of the distributions, additional differences are evident. For instance, cartwheel topspin motion is clearly preferred over cartwheel backspin motion for both surfaces at the two incidence angles studied, including the CF_3-SAM at $\theta_i = 30°$ (Figure 5c), which exhibits topspin−backspin symmetry when considering all of the CO flux (Figure 4c). In addition, Figure 5 shows that, for rotationally excited CO, cartwheel topspin motion is also more favored than corkscrew motions for both surfaces at both incident angles.

3. Stereodynamic Properties of CO with Initially Aligned/Oriented Collision Geometry. While there are clear trends in the final orientation and alignment of scattered CO molecules that approach the surface with a random collision geometry, we also find that the initial CO collision geometry has a significant effect on the outcome of the collision. To investigate this effect, we have integrated batches of trajectories in each of four different CO approach geometries for each of the four combinations of surface and incident angle studied in this work. Schematics of the initial collision geometries are given in Figure 6a. In the first two approaches, the nonrotating CO molecule is aligned with its bond parallel with the surface normal, and with either the O or C atom located closest to the surface; we will refer to these as O-end-on and C-end-on collision geometries, respectively. In the other two approaches, which we refer to as ||-side-on and ⊥-side-on, the CO bond is perpendicular with the surface normal. In the ||-side-on approach, the CO bond is aligned parallel to the $\mathbf{k}$ vector projection on the xy-plane, which in this work corresponds to the SAM surface plane. Analogously, in the ⊥-side-on approach, CO is aligned with its bond perpendicular to this projection. We give a summary of the energy transfer properties for these collisions in Table 3. The average final translational energy, $\langle E'_T \rangle$, values indicate that the initial collision geometry influences the translational energy transfer. Overall, the ||-side-on collision geometry results in larger final translational energy than the rest of the approaches, and this is especially evident for the CF_3-SAM surface and with a glancing angle of $\theta_i = 60°$. Under these conditions, we see that CO in a ||-side-on approach transfers significantly less collision energy than CO in a ⊥-side-on collision geometry. ||-side-on CO has its linear momentum directed along the $-z$ and $+x$ direction and its internuclear axis is aligned along the x-axis. ⊥-side-on CO also has its linear momentum directed along the $-z$ and $+x$ direction but the alignment of its internuclear axis along the y-axis makes it possible to interact with a larger region of the SAM than the ||-side-on approach, thereby enhancing energy transfer. This trend is backed by the substantially larger number of direct trajectories and smaller number of long-trapped trajectories for ||-side-on trajectories.

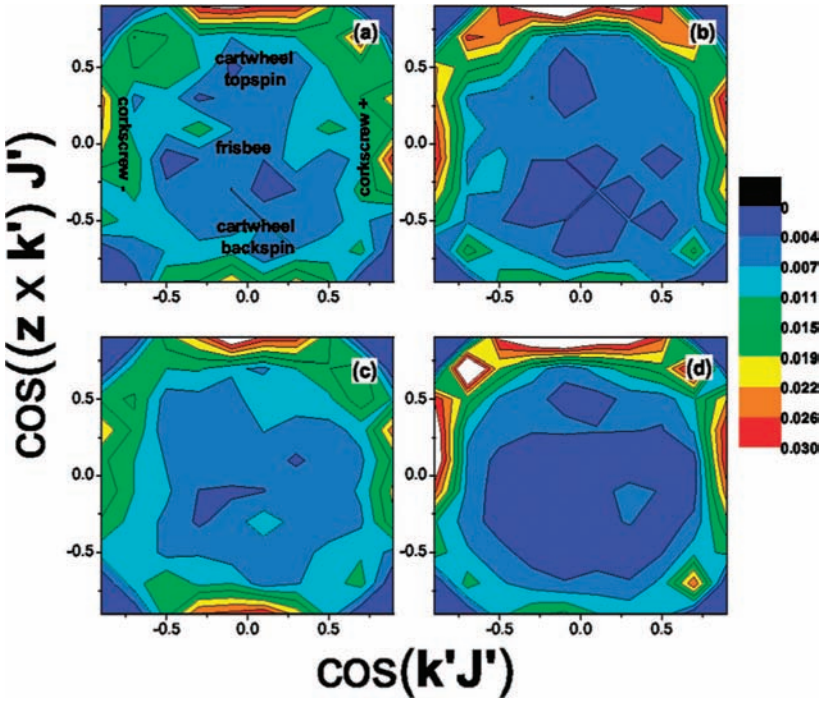

Figure 5. Probability contours of CO scattering with given $\mathbf{k}'\mathbf{J}'$ and $(\mathbf{z} \times \mathbf{k}')\mathbf{J}'$ angles in collisions with a CH_3-SAM (a, b), and a CF_3-SAM (c, d), at $E_{coll} = 60$ kJ·mol^{-1} and $v = 0$, $j = 0$. The graphs consider only trajectories in which CO results highly rotationally excited ($\mathbf{J}' \geq 20$). The angle of incidence is 30° for (a) and (c) and 60° for (b) and (d). Contours are drawn from zero probability (blue) to probability 0.03 (maroon) at 0.00375 steps. Labels in panel a indicate the location of the limiting rotational motions. White areas indicate probabilities larger than 0.03.

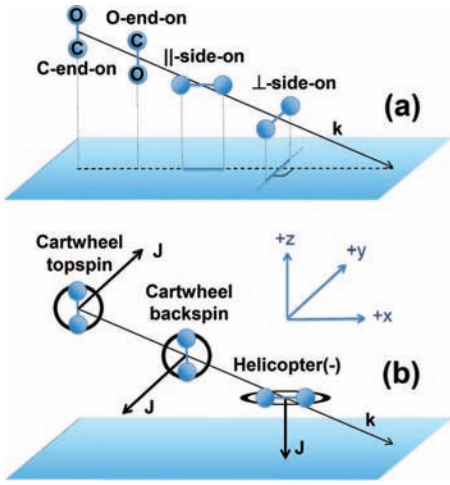

Figure 6. Schematic of the various (a) initial collision geometries explored in CO($j = 0$)/SAM calculations and (b) initial rotational motions explored in CO($j = 28$)/SAM calculations.

TABLE 3: Final CO Properties for Various Initial CO Collision Geometries in Collisions with CH_3- and CF_3-SAMs[a]

surface	approach	$\langle E'_T \rangle$[b]	$\langle E'_{ROT} \rangle$[c]	% direct[d]	% long[e]
			$\theta_i = 30°$		
CH_3-SAM	O-end-on	7.3	3.7	38.0	30.5
	C-end-on	7.1	4.2	38.2	30.5
	||-side-on	7.8	3.1	38.5	31.1
	⊥-side-on	7.5	3.1	39.1	30.9
CF_3-SAM	O-end-on	11.8	8.4	55.2	9.6
	C-end-on	13.6	6.9	68.0	7.3
	||-side-on	16.1	3.9	76.5	6.2
	⊥-side-on	10.2	2.9	63.5	13.2
			$\theta_i = 60°$		
CH_3-SAM	O-end-on	15.1	4.3	40.8	20.6
	C-end-on	14.8	4.7	42.7	21.1
	||-side-on	17.3	3.1	51.9	17.4
	⊥-side-on	15.8	3.3	47.9	20.0
CF_3-SAM	O-end-on	25.7	6.8	54.3	4.5
	C-end-on	26.4	6.6	62.7	2.9
	||-side-on	31.2	3.2	76.0	2.1
	⊥-side-on	22.8	2.8	61.8	8.4

[a] All trajectories calculated with $E_{coll} = 60$ kJ/mol, $v = 0$, $j = 0$. [b] Average final CO translational energy in kJ·mol^{-1}. [c] Average final CO rotational energy in kJ·mol^{-1}. [d] Percentage of trajectories experiencing only one turning point. [e] Percentage of trajectories that do not complete within 15 ps.

This result also suggests that thermal accommodation is favored for ⊥-side-on approach geometries.

Table 3 also shows the average final rotational energy of CO, $\langle E'_{ROT} \rangle$, for the four collision geometries considered in this work. Comparison of these rotational energies immediately shows a marked difference between those approaches in which CO is aligned parallel (end-on) or perpendicular (side-on) to the surface normal. As one may intuitively expect, end-on approaches result in larger rotational excitation of CO molecules in comparison to side-on approaches in glancing collisions. This effect is greatest at $\theta_i = 60°$, where final rotational energy of end-on approaches is more than double that of side-on approaches. This result emerges from the fact that while in side-on approaches both atoms collide with the SAM at the same time on average, in end-on approaches, only one of the atoms initially collides with the surface directly. This atom experiences a repulsion from the surface in a direction opposite to the direction of travel, which results in a torque and rotational excitation. It is also interesting to note that for a perfectly flat and smooth surface, side-on approaches would not result in rotational excitation if the forces acting on each of the atoms of the gas-phase rotor are identical. The fact that we see rotational excitation for side-on approaches in this work is therefore either an indication of the degree of corrugation of the SAM surfaces investigated in this work or an indication of large differences in the C/SAM vs O/SAM potential. While our previous work did reveal a slight

TABLE 4: Average Orientation and Alignment Moments of the Final Rotational Angular Momentum in Collisions of CO($v = 0, j = 0$) with CH_3- and CF_3-SAMs at $E_{coll} = 60$ kJ·mol^{-1}[a]

surface	approach	$\langle J'_x\rangle/\langle\|\mathbf{J}'\|\rangle$	$\langle 3J'^2_x\rangle/\langle\|\mathbf{J}'\|^2\rangle - 1$	$\langle J'_y\rangle/\langle\|\mathbf{J}'\|\rangle$	$\langle 3J'^2_y\rangle/\langle\|\mathbf{J}'\|^2\rangle - 1$	$\langle J'_z\rangle/\langle\|\mathbf{J}'\|\rangle$	$\langle 3J'^2_z\rangle/\langle\|\mathbf{J}'\|^2\rangle - 1$
				$\theta_i = 30°$			
CH_3-SAM	O-end-on	0.00 (−0.01)	0.05 (0.14)	0.17 (0.28)	0.23 (0.41)	−0.01 (−0.07)	−0.27 (−0.55)
	C-end-on	0.01 (0.05)	0.07 (0.09)	0.17 (0.34)	0.21 (0.37)	0.00 (0.01)	−0.28 (−0.48)
	∥-side-on	0.01 (−0.02)	−0.21 (−0.52)	0.01 (−0.04)	0.17 (0.26)	0.00 (0.00)	0.04 (0.25)
	⊥-side-on	−0.01 (−0.19)	0.06 (0.08)	0.04 (0.14)	−0.09 (−0.31)	0.01 (0.04)	0.04 (0.23)
CF_3-SAM	O-end-on	0.02 (0.03)	0.23 (0.25)	0.27 (0.37)	0.46 (0.61)	0.01 (0.01)	−0.69 (−0.86)
	C-end-on	0.02 (0.00)	0.12 (0.14)	0.30 (0.39)	0.46 (0.65)	0.00 (0.00)	−0.58(−0.78)
	∥-side-on	−0.01 (−0.06)	−0.44 (−0.55)	−0.14 (0.01)	0.35 (0.24)	0.02 (−0.06)	0.08 (0.30)
	⊥-side-on	0.00 (−0.04)	0.07 (0.20)	0.08 (0.19)	−0.27 (−0.39)	0.01 (−0.01)	0.20 (0.18)
				$\theta_i = 60°$			
CH_3-SAM	O-end-on	0.02 (−0.09)	−0.04 (−0.11)	0.27 (0.63)	0.36 (0.78)	0.00(−0.01)	−0.32 (−0.67)
	C-end-on	0.00 (0.03)	−0.07 (−0.15)	0.30 (0.61)	0.32 (0.82)	0.00 (0.00)	−0.25 (−0.67)
	∥-side-on	0.01 (0.06)	−0.17 (−0.30)	−0.08 (0.03)	0.28 (0.47)	−0.01 (−0.01)	−0.10 (−0.17)
	⊥-side-on	−0.01 (−0.03)	0.12 (−0.04)	0.10 (0.31)	−0.15 (−0.06)	−0.01 (−0.06)	0.03 (0.10)
CF_3-SAM	O-end-on	0.00 (0.00)	0.15 (−0.01)	0.41 (0.66)	0.49 (0.83)	0.01 (0.00)	−0.64 (−0.82)
	C-end-on	−0.01 (−0.02)	0.10 (−0.07)	0.38 (0.65)	0.40 (0.83)	0.00 (0.01)	−0.50 (−0.76)
	∥-side-on	0.01 (0.03)	−0.40 (−0.36)	−0.20 (0.03)	0.48 (0.50)	0.01 (−0.06)	−0.06 (−0.14)
	⊥-side-on	0.00 (−0.07)	0.11 (−0.04)	0.11 (0.34)	−0.31 (−0.02)	0.01 (0.04)	0.20 (0.06)

[a] Values between parentheses correspond to averages over trajectories in which CO results with a final rotational quantum number of 20 or larger.

difference in OC vs CO approach geometry in the CO/SAM intermolecular potentials,[36] the difference is quite minor in comparison to the collision energy used in this work. Therefore, rotational excitation in side-on CO/SAM collisions is mainly due to surface corrugation.

Further insight into the dynamics of initially aligned CO molecules scattering from SAM surfaces can be gained by examining the orientation and alignment of the final rotational angular momentum. Table 4 displays calculated orientation and alignment moments of the final rotational angular momentum vector as decribed before. We first note that, in contrast with the near-zero moments obtained for random collision geometry in Table 2, we observe significantly nonzero values in a number of moments when the molecules impinge with specifically aligned/oriented collision geometries. For the end-on approaches, large negative $3J'^2_z/|\mathbf{J}'|^2 - 1$ values coupled with large positive $3J'^2_y/|\mathbf{J}'|^2 - 1$ values indicate a strong preference for cartwheel alignment. Substantial positive $J'_y/|\mathbf{J}'|$ values further indicate that topspinning motion is preferred. This result bodes well with the expectation for a rotor traveling in the $+x$, $-z$ direction and impinging end-on upon a corrugated surface that exerts a force in the $-x$, $+z$ direction only on the atom that is closest to the surface. In this model, pure cartwheel topspin motion should be expected. Therefore, the result of $3J'^2_y/|\mathbf{J}'|^2 - 1$ being less than $+2.0$ and of $J'_y/|\mathbf{J}'|$ being less than $+1.0$ indicates forces acting in the y-direction or, in other words, surface corrugation orthogonal to the direction of travel. The finding that the degree of orientation and aligment is larger for the CF_3-SAM surface than for the CH_3-SAM surface can be explained as due to larger effective corrugation for the lighter surface.

Examination of the data for the side-on approaches enables further understanding of the effect of a corrugated surface on the orientation and alignment of the rotational angular momentum of a scattering diatomic molecule. In a flat and smooth model surface, with spherically symmetric forces about the surface normal, no rotational excitation should be expected in side-on collisions (in the limit of a homonuclear diatomic). Therefore, the presence of rotational excitation in our calculations must be due to surface corrugation, as mentioned above. In the case of a corrugated surface, if there were no forces orthogonal to the direction of travel, rotation with perfect cartwheel alignment should be expected for ∥-side-on collisions, and no rotational excitation (and therefore no alignment) would be possible for ⊥-side-on collisions. Tangential forces that emerge as a result of surface corrugation change these expected limiting trends. For instance, in a corrugated surface, tangential forces acting preferentially on one of the atoms will tend to promote helicopter motion in ∥-side-on collisions at the expense of cartwheel motion. Likewise, surface forces opposite to the direction of travel for a ⊥-side-on collision acting on only one of the atoms will also tend to produce helicopter motion. This is exactly what we see in the alignment and orientation moments of Table 4 for the two side-on approaches explored. For the ∥-side-on collision geometry, there is a tendency toward cartwheel alignment (positive values of $3J'^2_y/|\mathbf{J}'|^2 - 1$), which increases in molecules that are highly rotationally excited. However, cartwheel alignment is not perfect, which, as described before, is indicative of surface corrugation. The $3J'^2_y/|\mathbf{J}'|^2 - 1$ values are larger for the CF_3-SAM than for the CH_3-SAM, which reinforces the idea that the lighter surface is more corrugated. Interestingly, helicopter motion is also present for highly rotationally excited CO impinging in ∥-side-on collision geometry, further suggesting that strong surface forces orthogonal to the direction of travel act preferentially on one of the atoms. Regarding ⊥-side-on collisions, we see some tendency toward helicopter alignment from the positive values of the $3J'^2_z/|\mathbf{J}'|^2 - 1$ moment, which contrasts with the absence of cartwheel alignment (negative $3J'^2_y/|\mathbf{J}'|^2 - 1$ moments). Helicopter motion in ⊥-side-on collisions is again proof of unequal in-plane forces on the two atoms of CO.

B. Collision Dynamics of CO in the $v = 0, j = 28$ State. The above discussion has focused on the stereodynamics of collisions of rotationally cold CO molecules with model organic surfaces. In the following, we turn our attention to collisions in which CO is initially rotationally excited. The presence of initial rotational excitation enables us to select the type of rotational motion of the impinging CO prior to collision and to investigate the effect of alignment and orientation of the initial rotational angular momentum on energy transfer and the mechanism of the collisions.

Our study is based on batches of trajectories of CO scattering from CH_3- and CF_3-SAM surfaces with $\theta_i = 30°$ or 60° and

TABLE 5: Energy Transfer Properties in Collisions of CO($v = 0, j = 28$) with CH_3- and CF_3-SAMs[a]

surface	initial motion	$\langle E'_T \rangle^b$	$\langle E'_{ROT} \rangle^c$	% direct[d]	% long[e]
			$\theta_i = 30°$		
CH_3-SAM	random	9.0	6.8	43.8	25.7
	cartwheel topspin	9.7	6.8	45.8	24.5
	cartwheel backspin	8.8	7.5	43.3	25.5
	helicopter	9.3	7.9	44.4	24.5
CF_3-SAM	random	19.0	11.6	78.2	4.2
	cartwheel topspin	20.1	12.0	77.8	3.7
	cartwheel backspin	17.1	13.5	69.3	6.4
	helicopter	18.7	14.6	78.8	4.3
			$\theta_i = 60°$		
CH_3-SAM	random	20.4	9.2	53.2	14.4
	cartwheel topspin	23.6	7.2	55.5	11.1
	cartwheel backspin	18.3	7.8	53.0	15.6
	helicopter	20.5	12.0	53.8	13.6
CF_3-SAM	random	34.5	12.6	75.6	1.4
	cartwheel topspin	37.7	10.0	73.8	0.9
	cartwheel backspin	32.0	11.4	72.1	1.2
	helicopter	33.8	16.4	75.0	1.1

[a] 60 kJ·mol^{-1} collision energy. [b] Average final CO translational energy in kJ·mol^{-1}. [c] Average final CO rotational energy in kJ·mol^{-1}. [d] Percentage of trajectories experiencing only one turning point. [e] Percentage of trajectories in which CO does not desorb the surface after 15 ps.

$E_{coll} = 60$ kJ·mol^{-1}. The CO was initially started in the $v = 0$, $j = 28$ state and with various initial alignments and orientations, which include cartwheel topspin, cartwheel backspin, helicopter(−), and random (see Figure 6b). Cartwheel topspin and backspin motions are analogous to those described in Figure 2, with the only difference being that the initial rotational angular momentum **J** is parallel to the **z** × **k** vector (where **k** is the initial center-of-mass velocity vector of CO) instead of to the **z** × **k′** vector in Figure 2. Helicopter(−) refers to the initial rotational motion in which CO approaches the surface rotating in a plane parallel to the SAM surface plane, with the initial rotational angular momentum pointing toward the surface. Calculations with molecules having initial helicopter motion but with an orientation such that the rotational angular momentum points away from the surface (helicopter(+)) gave results identical to those reported here for helicopter(−) and will not be reported. Due to this insensitivity of the dynamics to the handedness of the initial helicopter rotation, we will refer to helicopter(−) simply as helicopter hereafter.

1. Energy Transfer. Table 5 shows energy transfer results for collisions of initially rotationally excited CO with the CH_3- and CF_3-SAM surfaces for both 30° and 60° incident angles. The average final translational energy, $\langle E'_T \rangle$, values indicate that the type of initial rotational motion has only a moderate effect on the final translational energy of CO. The largest differences in the four initial rotational motions investigated occur between the topspin and backspin cartwheel initial orientations. Collisions in which CO impinges having a cartwheel topspin rotational motion result in CO leaving the surface slightly faster than those in which CO is moving with cartwheel backspin motion, particularly for grazing incidence (60°). This result is rationalized by the fact that in topspin (backspin) motion, the atom closer to the SAM surface (and hence the atom which will participate in collision first) has its tangential rotational momentum pointed antiparallel (parallel) to the center-of-mass momentum in the *xy*-plane. For a backspinning molecule, this acts to increase the collisional momentum, yielding a harder hit with the surface and enhancing translational energy transfer to the surface. In the topspin case, the tangential rotational momentum decreases the collisional momentum, resulting in a softer encounter with the surface and decreased energy transfer. Irrespective of the individual values for the various initial rotational motions, the well-known trend that an increase in the incident angle and in the surface mass both impair translational energy transfer seen before for CO($v = 0, j = 0$) holds here for CO($v = 0$, j = 28) collisions.

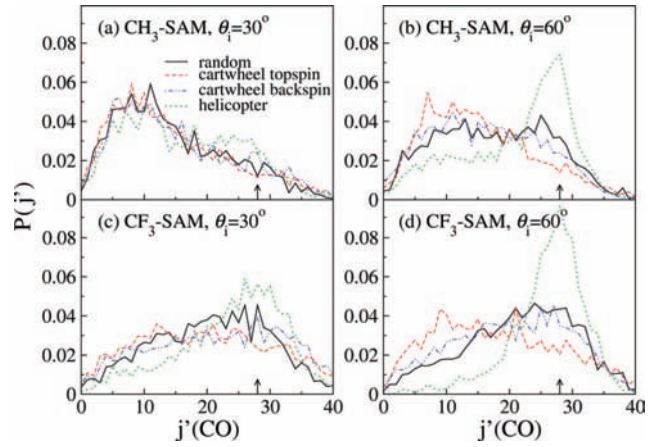

Figure 7. Final rotational distributions for CO scattering with either $\theta_i = 30°$ (a and c) or $\theta_i = 60°$ (b and d) from the (a, b) CH_3- and (c, d) CF_3-SAM surfaces having various initial rotational motions. CO is initially in the $j = 28$ state, as indicated by the arrows in the figure.

Table 5 also shows the average final rotational energy of CO, $\langle E'_{ROT} \rangle$. These values are smaller than the initial CO rotational energy (18.7 kJ·mol^{-1} for $j = 28$), implying a net loss of rotation during the collisions for all four combinations of surface and incident angle studied. This loss in rotation is caused by the torques elicited by the surface on the molecule upon collision, which tend to occur in a direction opposite to the molecular rotational motion. Comparison of the final rotational energy of CO for the various initial rotational motions studied reveals that helicopter motion is the most effective in preserving the initial rotation. This result can be understood by invoking a simplistic flat, smooth surface model and predicting deviations from that model when corrugation is present. The presence of only normal forces in a flat, smooth surface would permit a molecule scattering with initial helicopter motion to retain all of its rotational angular momentum, since there are no forces in the direction of rotation. Changes in the rotational angular momentum of a molecule approaching a surface with helicopter motion are therefore an indication of the degree of tangential forces. On the other hand, initial cartwheel rotations occur in a plane including the surface-normal axis and, therefore, would be arrested in collision with this idealized surface even if there is no corrugation. The average final rotational energies in Table 5 and the rotational distributions in Figure 7 show the expected result that the amount of rotational excitation in helicopter CO is larger than that in any of the other approaches examined.

Mechanistically, we see that initial rotational excitation results in both a larger percentage of direct processes and a smaller percentage of trajectories that trap on the surface for a long time when compared with the results obtained with rotationless CO in Table 1. It therefore seems that initial rotational excitation impairs slightly the gas/surface attractions that elicit nondirect processes, thereby promoting direct collisions.

2. Alignment and Orientation of the Final CO Rotational Angular Momentum. Table 6 shows calculated orientation and alignment moments of the final rotational angular momentum with respect to the Cartesian reference frame defined in this

TABLE 6: Average Orientation and Alignment Moments of the Final Rotational Angular Momentum in Collisions of CO(v = 0, j = 28) with CH_3- and CF_3-SAMs at E_{coll} = 60 kJ·mol^{-1} [a]

surface	θ_i	$\langle J'_x\rangle/(\|\mathbf{J}'\|)$	$\langle 3J'^2_x\rangle/(\|\mathbf{J}'\|^2) - 1$	$\langle J'_y\rangle/(\|\mathbf{J}'\|)$	$\langle 3J'^2_y\rangle/(\|\mathbf{J}'\|^2) - 1$	$\langle J'_z\rangle/(\|\mathbf{J}'\|)$	$\langle 3J'^2_z\rangle/(\|\mathbf{J}'\|^2) - 1$
CH_3-SAM	30	0.00 (−0.01)	−0.04 (−0.09)	0.00 (−0.02)	−0.03 (−0.08)	0.00 (0.02)	0.07 (0.17)
	60	0.00 (0.01)	−0.03 (−0.07)	0.00 (0.00)	−0.08 (−0.14)	−0.01 (0.00)	0.10 (0.21)
CF_3-SAM	30	−0.01 (−0.01)	−0.05 (−0.08)	0.02 (0.01)	−0.05 (−0.09)	0.01 (0.01)	0.09 (0.17)
	60	−0.01 (−0.02)	−0.06 (−0.11)	0.01 (0.02)	−0.05 (−0.10)	0.01 (0.01)	0.11 (0.21)

[a] Values in parentheses correspond to averages over trajectories in which CO results with a final rotational quantum number of 20 or larger.

work for collisions of rotationally excited CO (j = 28) with the CH_3- and CF_3-SAMs. There are several differences between the values in Table 6 and those obtained for rotationless CO (Table 2). First, the presence of a modest alignment along the y-axis (cartwheel rotation) seen in Table 2 is not present for CO(j = 28), even when we examine trajectories that retain a high level of rotational excitation. Instead, the values of $3J'^2_y/|\mathbf{J}'|^2 - 1$ are slightly negative, which indicates a slight tendency to rotate in a plane parallel to the y-axis (i.e., there is no tendency toward cartwheel rotation). This tendency increases when CO emerges rotationally excited, as indicated by the values in parentheses in Table 6. Second, there seems to be a small tendency to rotate in a plane perpendicular to the z-axis (helicopter motion), as indicated by the slightly positive values of the $3J'^2_z/|\mathbf{J}'|^2 - 1$ moment. Examination of the orientation moment in this axis ($J'_z/|\mathbf{J}'|$) reveals that the rotational motion does not have a dominant handedness (i.e., the average values of the orientation moment $J'_z/|\mathbf{J}'|$ are close to 0.0).

The conclusion stemming from Table 6 is that initial rotational excitation removes the slight tendency toward cartwheel topspin rotation seen in collisions with CO(j = 0) and instead favors a helicopter motion. To illustrate this transition from a preference for rotation in a plane perpendicular to the SAM surface for CO(j = 0) to in-plane rotation for CO(j = 28), we show in Figure 8 the probability distribution of the angle formed between the surface normal (**z**) and the final rotational angular momentum vector (**J′**) for CO collisions with the CF_3-SAM at 60 kJ·mol^{-1} and θ_i =30° with j = 0 or 28. The figure only includes trajectories in which CO results with a rotational quantum number of 20 or larger. In perfect helicopter motion, the cosine of this angle is either −1.0 or +1.0, depending on the orientation of **J′**. On the other hand, in perfect cartwheel rotation, cos(**J′z**) = 0.0. The figure clearly shows that initially rotationless CO tends to rotate in a plane perpendicular to the SAM surface plane after collision, while CO initially in j = 28 favors rotation in the SAM surface plane. The preference for helicopter over cartwheel motion for initially rotationally excited CO can be explained as follows. For the j = 0 case, molecules generally require an end-on molecular geometry to yield high (j' > 20) rotational excitation, as is evidenced by the data in Table 3. Additionally, we have shown in Table 4 that molecules initially in an end-on approach geometry preferentially scatter with a cartwheel alignment. Although rotationally cold molecules whose approach geometry yields alignments other than cartwheel contribute to the trace in Figure 8, their contribution is small, as fewer molecules obtain the necessary rotational momentum (j' ≥ 20) to be included in the distribution than those exhibiting cartwheel alignment. Analogously, the reverse argument explains the behavior for the j = 28 case in Figure 8. Deactivation of the initial rotation is greatest when CO impinges with cartwheel motion. This effect will act to depopulate cartwheel alignment from the cos(**J′z**) distribution for j = 28. On the other hand, CO(j = 28) molecules impinging upon the surface with helicopter motion retain their high level of initial rotation (see Figure 7 and Table 5) and conserve population of this alignment in the distribution.

We now turn our attention to the stereodynamics of collisions of CO(j = 28) in which the *initial* rotational angular momentum is perfectly aligned and oriented in helicopter, cartwheel topspin, and cartwheel backspin motions (see Figure 6b). To determine the correlation between initial and final CO angular momentum, we plot in Figure 9 cos(**JJ′**) probability distributions as a function of incident angle for the various initial CO rotational motions examined here. In the figure, population toward the +1.0 limiting value therefore corresponds to trajectories in which the CO rotational angular momentum alignment and orientation do not vary during collision. On the other hand, population toward −1.0 corresponds to trajectories in which

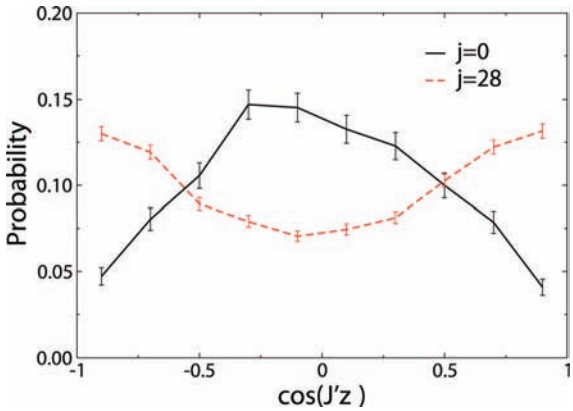

Figure 8. Probability distributions of the angle formed between the final rotational angular momentum and the surface normal in collisions of CO(v = 0, j) with a CF_3-SAM surface at E_{coll} = 60 kJ·mol^{-1}, θ_i = 30°, and with the initial rotational state of CO being 0 or 28. The distributions have been calculated with trajectories in which the final quantum state of CO is 20 or larger.

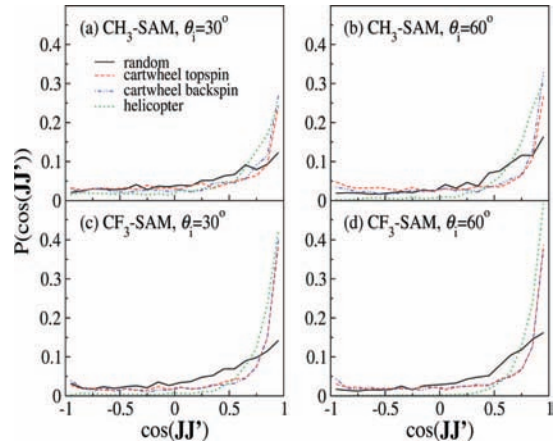

Figure 9. Calculated cos(**JJ′**) distributions as a function of initial rotational motion for CO scattering with either θ_i =30° (a and c) or θ_i 60° (b and d) from the (a, b) CH_3- and (c, d) CF_3-SAM surfaces. The CO is initially in the v = 0, j = 28 state.

TABLE 7: Orientation and Alignment Factors between Initial and Final Rotational Angular Momentum in Collisions of CO($v = 0, j = 28$) with CH_3- and CF_3-SAMs[a]

surface	initial motion	$\langle\cos(\mathbf{JJ}')\rangle$	$\langle 3\cos^2(\mathbf{JJ}') - 1\rangle$
		$\theta_i = 30°$	
CH_3-SAM	random	0.28 (0.65)	0.21 (0.58)
	cartwheel topspin	0.31 (0.84)	0.44 (1.33)
	cartwheel backspin	0.40 (0.85)	0.58 (1.37)
	helicopter	0.51 (0.80)	0.64 (1.03)
CF_3-SAM	random	0.35 (0.66)	0.31 (0.59)
	cartwheel topspin	0.54 (0.90)	0.86 (1.52)
	cartwheel backspin	0.54 (0.86)	0.93 (1.37)
	helicopter	0.77 (0.88)	1.08 (1.35)
		$\theta_i = 60°$	
CH_3-SAM	random	0.42 (0.61)	0.31 (0.48)
	cartwheel topspin	0.31 (0.86)	0.59 (1.45)
	cartwheel backspin	0.45 (0.90)	0.72 (1.53)
	helicopter	0.71 (0.84)	0.86 (1.21)
CF_3-SAM	random	0.46 (0.70)	0.39 (0.71)
	cartwheel topspin	0.51 (0.93)	0.84 (1.65)
	cartwheel backspin	0.49 (0.86)	0.84 (1.43)
	helicopter	0.84 (0.88)	1.23 (1.37)

[a] 60 kJ·mol^{-1} collision energy. Values in parentheses correspond to averages over trajectories in which CO results with a final rotational quantum number of 20 or larger.

the CO rotational angular momentum remains aligned but changes orientation (becomes antiparallel with respect to the initial momentum) during the collision. To help quantify the differences between the various initial motions, we show in Table 7 average values of $\cos(\mathbf{JJ}')$, which indicate the degree of orientation of the vectors, and of $3\cos^2(\mathbf{JJ}') - 1$, which quantify their alignment. Values of $\langle\cos(\mathbf{JJ}')\rangle$ close to $+1.0(-1.0)$ indicate a large degree of parallel(antiparallel) orientation. On the other hand, values of $\langle 3\cos^2(\mathbf{JJ}') - 1\rangle$ close to $+2.0$ suggest a large degree of alignment, and values close to -1.0 are indicative of poor alignment between the $\mathbf{J}$ and $\mathbf{J}'$ vectors.

Some general trends can be drawn from the data in Figure 9 and Table 7. Regarding alignment, initial random rotational motion shows significantly poorer alignment of the $\mathbf{JJ}'$ vectors than any of the other initial rotations for collisions on both surfaces at both angles. This result likely emerges from the ability of random rotation to explore a broader region of the anisotropic gas/surface potential, which scrambles the initial rotational motion. Initial helicopter motion shows the best $\mathbf{JJ}'$ alignment, which is consistent with the notion that the absence of rotational motion in the surface-normal direction helps preserve the rotational angular momentum in this approach. Backspin and topspin motions provide $\mathbf{JJ}'$ alignments intermediate between random and helicopter initial motions, with backspin $\langle 3\cos^2(\mathbf{JJ}') - 1\rangle$ values being generally larger than topspin. Regarding orientation, helicopter motion also shows the largest value of the orientation moment calculated here, which again is a consequence of the lower probability for this motion to experience surface forces opposite to the direction of rotation with respect to other initial motions. However, a difference with the alignment trends described before is that random initial motion does not always provide the poorest degree of orientation. Instead, random and both cartwheel motions have comparable $\langle\cos(\mathbf{JJ}')\rangle$ values for both surfaces and both angles, and these values are clearly smaller than those for helicopter motion. Finally, comparison between the surfaces shows that the CF_3-SAM surface promotes retention of the initial orientation and alignment of the rotational angular momentum vector, particularly in collisions at $\theta_i = 60°$. The dependence of the $\mathbf{JJ}'$ correlation with the incident angle and surface seems to be tied with the mechanism governing the collisions. The data in Table 5 show that direct collisions are favored at larger incident angles and with the more massive surface. This result nicely corroborates the intuitive trend that direct collisions, for which the gas/surface interaction is brief, better conserve initial alignment and orientation than nondirect collisions. In addition, the larger corrugation of the CH_3-SAM acts to scramble the initial rotational angular momentum to a larger extent than in the effectively smoother CF_3-SAM surface.

IV. Concluding Remarks

A theoretical study of CO collisions with regular and ω-fluorinated alkanethiolate monolayers has been presented with a focus on understanding the collision stereodynamics. Rotationless CO scattering with initial random collision geometry from the CH_3- and CF_3-SAMs gains rotational excitation, but the alignment and orientation of the resulting rotational angular momentum are weak. Both alignment and orientation become more apparent when the analysis is restricted to trajectories in which CO gains large amounts of rotational excitation. The expected cartwheel topspin motion is evident in our analysis, but there is also a non-negligible contribution from unhanded corkscrew motion. The fact that cartwheel topspin motion is more prominent in collisions with the CF_3-SAM than with the CH_3-SAM suggests that the lighter SAM is effectively more corrugated than the terminally fluorinated SAM.

Examination of the dynamics of various end-on and side-on initial approach geometries of rotationless CO indicate large corrugation of the model organic surfaces used in this work. The trend that end-on collisions result in more rotational excitation and stronger cartwheel topspin in the CF_3-SAM than in the CH_3-SAM provides further evidence of the larger effective corrugation of the latter surface.

Initial rotational excitation in CO scattering with random molecular orientation from the surfaces removes the tendency for final cartwheel topspin motion seen when CO impinges on the surfaces without rotational excitation. Instead, unhanded helicopter motion appears to be present in trajectories in which CO ends up rotationally excited after the collision. This result is rationalized as emerging from the better conservation of rotational angular momentum in gas/surface collisions in which CO is initially rotating in the surface plane. Conservation of initial CO rotational angular momentum is especially strong in the CF_3-SAM, reinforcing the notion that this surface is effectively smoother than the CH_3-SAM surface.

While this study has focused on relatively high energy collisions of a weakly polar diatomic molecule with a surface, future studies will be aimed at understanding how stronger gas/surface forces, such as hydrogen bonding, govern the collision stereodynamics. In particular, if the gas/surface forces are comparable to the collision and initial rotational energy, steering effects that are not appreciable in the CO/SAM systems under the high-energy conditions of this work will likely change the dynamics and stereodynamics of the gas/organic surface systems studied until now.

Acknowledgment. This work has been supported by NSF Grant No. CHE-0547543 and AFOSR Grant No. FA9550-06-1-0165. D.T. is a Cottrell Scholar of Research Corporation.

Supporting Information Available: Animations of various representative trajectories that exhibit the different stereodynamic motions examined in this article. This material is available free of charge via the Internet at http://pubs.acs.org/.

References and Notes

(1) Solomon, S. *Rev. Geophys.* **1999**, *37*, 275.
(2) Hanson, D. R.; Lovejoy, E. R. *J. Phys. Chem.* **1996**, *100*, 6397.
(3) Troya, D.; Schatz, G. C. *Int. Rev. Phys. Chem.* **2004**, *23*, 341.
(4) Minton, T. K.; Tagawa, M.; Nathanson, G. M. *J. Spacecr. Rockets* **2004**, *41*, 389.
(5) Ellison, G. B.; Tuck, A. F.; Vaida, V. *J. Geophys. Res. Atmos.* **1999**, *104*, 11633.
(6) Saecker, M. E.; Govoni, S. T.; Kowalski, D. V.; King, M. E.; Nathanson, G. M. *Science* **1991**, *252*, 1421.
(7) King, M. E.; Nathanson, G. M.; Hanning-Lee, M. A.; Minton, T. K. *Phys. Rev. Lett.* **1993**, *70*, 1026.
(8) Saecker, M. E.; Nathanson, G. M. *J. Chem. Phys.* **1993**, *100*, 3999.
(9) Nathanson, G. M. *Annu. Rev. Phys. Chem.* **2004**, *55*, 231.
(10) Day, B. S.; Morris, J. R. *J. Phys. Chem. B* **2003**, *107*, 7120.
(11) Day, B. S.; Shuler, S. F.; Ducre, A.; Morris, J. R. *J. Chem. Phys.* **2003**, *119*, 8084.
(12) Day, B. S.; Morris, J. R. *J. Chem. Phys.* **2005**, *122*, 234714.
(13) Day, B. S.; Morris, J. R.; Troya, D. *J. Chem. Phys.* **2005**, *122*, 214712.
(14) Day, B. S.; Morris, J. R.; Alexander, W. A.; Troya, D. *J. Phys. Chem. A* **2006**, *110*, 1319.
(15) Alexander, W. A.; Day, B. S.; Moore, H. J.; Lee, T. R.; Morris, J. R.; Troya, D. *J. Chem. Phys.* **2008**, *128*, 014713.
(16) Tasic, U.; Day, B. S.; Yan, T.-Y.; Morris, J. R.; Hase, W. L. *J. Phys. Chem. C* **2008**, *112*, 476.
(17) Vazquez, S. A.; Morris, J. R.; Rahaman, A.; Mazyar, O. A.; Vayner, G.; Addepalli, S. V.; Hase, W. L.; Martinez-Nunez, E. *J. Phys. Chem. A* **2007**, *111*, 12785.
(18) Bosio, S. B. M.; Hase, W. L. *J. Chem. Phys.* **1997**, *107*, 9677.
(19) Yan, T.-Y.; Hase, W. L. *Phys. Chem. Chem. Phys.* **2000**, *2*, 901.
(20) Yan, T.-Y.; Isa, N.; Gibson, K. D.; Sibener, S. J.; Hase, W. L. *J. Phys. Chem. A* **2003**, *107*, 10600.
(21) Isa, N.; Gibson, K. D.; Yan, T.-Y.; Hase, W. L.; Sibener, S. J. *J. Chem. Phys.* **2004**, *120*, 2417.
(22) Gibson, K. D.; Isa, N.; Sibener, S. J. *J. Chem. Phys.* **2003**, *119*, 13083.
(23) Gibson, K. D.; Isa, N.; Sibener, S. J. *J. Phys. Chem. A* **2006**, *110*, 1469.
(24) Fogarty, D. P.; Kautz, N. A.; Kandel, S. A. *Surf. Sci.* **2007**, *601*, 2117.
(25) Fogarty, D. P.; Kandel, S. A. *J. Chem. Phys.* **2006**, *125*, 174710.
(26) Troya, D.; Schatz, G. C. *J. Chem. Phys.* **2004**, *120*, 7696.
(27) Troya, D.; Schatz, G. C. A QM/MM model for hyperthermal O(^{3}P) collisions with hydrocarbon self-assembled monolayers. In *Proceedings of the 9th International Symposium on Materials in a Space Environment*; European Space Agency, SP-540, 2003, p 121.
(28) Allan, M.; Bagot, P. A. J.; Westacott, R. E.; Costen, M. L.; McKendrick, K. G. *J. Phys. Chem. C* **2008**, *112*, 1524.
(29) Allan, M.; Bagot, P. A. J.; Costen, M. L.; McKendrick, K. G. *J. Phys. Chem. C* **2007**, *111*, 14833.
(30) King, M. E.; Saecker, M. E.; Nathanson, G. M. *J. Chem. Phys.* **1994**, *101*, 2539.
(31) Cohen, S. R.; Naaman, R.; Sagiv, J. *Phys. Rev. Lett.* **1987**, *58*, 1208.
(32) Cohen, S. R.; Naaman, R.; Sagiv, J. *J. Chem. Phys.* **1988**, *88*, 2757.
(33) Bennett, M. E.; Alexander, W. A.; Lu, J. W.; Troya, D.; Morris, J. R. *J. Phys. Chem. C* **2008**, *112*, 17272.
(34) Kenyon, A. J.; McCaffery, A. J.; Quintella, C. M.; Zidan, M. D. *J. Chem. Soc., Faraday Trans.* **1993**, *89*, 3877.
(35) Kenyon, A. J.; McCaffery, A. J.; Quintella, C. M.; Zidan, M. D. *Faraday Discuss.* **1993**, *96*, 245.
(36) Alexander, W. A.; Morris, J. R.; Troya, D. *J. Chem. Phys.* **2009**, in press.
(37) Perkins, B. G., Jr.; Haber, T.; Nesbitt, D. J. *J. Phys. Chem. B* **2005**, *109*, 16396.
(38) Perkins, B. G., Jr.; Nesbitt, D. J. *J. Phys. Chem. B* **2006**, *110*, 17126.
(39) Perkins, B. G., Jr.; Nesbitt, D. J. *J. Phys. Chem. A* **2007**, *111*, 7420.
(40) Perkins, B. G., Jr.; Nesbitt, D. J. *Proc. Natl. Acad. Sci.U.S.A.* **2008**, *105*, 12684.
(41) Perkins, B. G., Jr.; Nesbitt, D. J. *J. Phys. Chem. B* **2008**, *112*, 507.
(42) Martinez-Nunez, E.; Rahaman, A.; Hase, W. L. *J. Phys. Chem. C* **2007**, *111*, 354.
(43) Lohr, J. R.; Day, B. S.; Morris, J. R. *J. Phys. Chem. B* **2005**, *109*, 15469.
(44) Lohr, J. R.; Day, B. S.; Morris, J. R. *J. Phys. Chem. A* **2006**, *110*, 1645.
(45) Bagot, P. A. J.; Waring, C.; Costen, M. L.; McKendrick, K. G. *J. Phys. Chem. C* **2008**, *112*, 10868.
(46) Saecker, M. E.; Nathanson, G. M. *J. Chem. Phys.* **1993**, *99*, 7056.
(47) Hanisco, T. F.; Yan, C.; Kummel, A. C. *J. Vac. Sci. Technol., A* **1993**, *11*, 2090.
(48) Hanisco, T. F.; Yan, C.; Kummel, A. C. *J. Chem. Phys.* **1992**, *97*, 1484.
(49) Kimman, J.; Rettner, C. T.; Auerbach, D. J.; Barker, J. A. *Phys. Rev. Lett.* **1986**, *57*, 2053.
(50) Rettner, C. T.; Kimman, J.; Auerbach, D. J. *J. Chem. Phys.* **1991**, *94*, 734.
(51) Jacobs, D. C.; Kolasinski, K. W.; Shane, S. F.; Zare, R. N. *J. Chem. Phys.* **1989**, *91*, 3182.
(52) Masson, D. P.; Hanisco, T. F.; Nichols, W. L.; Yan, C.; Kummel, A. C.; Tully, J. C. *J. Chem. Phys.* **1994**, *101*, 3341.
(53) Sitz, G. O.; Kummel, A. C.; Zare, R. N. *J. Chem. Phys.* **1988**, *89*, 2558.
(54) Sitz, G. O.; Kummel, A. C.; Zare, R. N.; Tully, J. C. *J. Chem. Phys.* **1988**, *89*, 2572.
(55) Jorgensen, W. L.; Madura, J. D.; Swenson, C. J. *J. Am. Chem. Soc.* **1984**, *106*, 6638.
(56) Jorgensen, W. L.; Tirado-Rives, J. *J. Am. Chem. Soc.* **1988**, *118*, 11225.
(57) Watkins, E. K.; Jorgensen, W. L. *J. Phys. Chem. A* **2001**, *105*, 4118.
(58) Hautman, J.; Klein, M. L. *J. Chem. Phys.* **1989**, *91*, 4994.
(59) Alexander, W. A.; Troya, D. *J. Phys. Chem. A* **2006**, *110*, 10834.
(60) Ponder, J. W.; Richards, F. M. *J. Comput. Chem.* **1987**, *8*, 1016.
(61) Hase, W. L.; Duchovic, R. J.; Hu, X.; Komornicki, A.; Lim, K. F.; Lu, D. h.; Peslherbe, G. H.; Swamya, K. N.; Linde, S. R. V.; Varandas, A.; et al. *Quantum Chem. Program Exchange Bull.* **1996**, *16*, 671.
(62) Hanisco, T. F.; Yan, C.; Kummel, A. C. *J. Phys. Chem.* **1992**, *96*, 2982.
(63) Kummel, A. C.; Sitz, G. O.; Zare, R. N.; Tully, J. C. *J. Chem. Phys.* **1988**, *89*, 6947.
(64) Jacobs, D. C.; Zare, R. N. *J. Chem. Phys.* **1989**, *91*, 3196.
(65) Mayne, H. R.; Kuan, C.-Y.; Wolf, R. J. *Chem. Phys. Lett.* **1987**, *140*, 520.

JP810557M